,

INVESTIGATING FUNCTIONAL PROPERTIES OF PdO AS A COMPONENT OF FUEL CELL MATERIALS

by

MULUGETA AREGAY G.

THESIS

SUMITTED TO THE DEPARTMENT OF PHYSICS

FOR FULFILLMENT OF THE REQUIREMENTS FOR THE DEGREE OF

MASTER OF SCIENCE

IN PHYSICS

AT THE

COLLEGE OF NATURAL SCIENCES

ADDIS ABABA UNIVERSITY

ADDIS ABABA, ETHIOPIA

Advisor: Kenate Nemera(PhD)

Co-Advisor: Lemi Demeyu(PhD)

Saturday 1st July, 2017

Dr. Kenate Nemera Nigussa	Date, Signature
Dr. Lemi Demeyu	Date, Signature
Dr. Tatek Yirgu	Date, Signature
Dr. Mulugeta Bekele	Date, Signature

Declaration

I declare that the thesis hereby submitted to the Addis Ababa University (AAU) for the degree of Master of Science has not been submitted by me for a degree at this or any other university, that it is my own work both in design and execution, and that all material contained herein has been duly acknowledged.

Mulugeta Aregay Date

Contents

Acknowledgement

I would like to thank Dr. Kenate Nemera for advising me and being patient and supportive throughout my graduate studies. I also acknowledge the help and constructive idea to my co-advisor Dr. Lemi Demeyu. I also acknowledge financial support for my studies provided by Addis Ababa University, Computational and Natural Science Faculity, Physics department. I also acknowledge Kotebe Metropolitan University for providing me scholarship to study physics at AAU.

I would also like to thank my friend, Sefiw Gebre for supporting me in material(lap top) throughout the study year.

And finally, I would like to thank my wife; Tizita Sebsibe, my daughter; Gelila Mulugeta and my son; Noah Mulugeta for being there for me always and helping me throughout my whole life, I wouldn't be able to be where I am without all of your continuous support. Thank you.

Mulugeta Aregay

Saturday 1st July, 2017Acknowledgement

List of Figures

List of Tables

Abstract

In this work, polymorphic models of the structures of PdO is considered. We used a relevant quantum mechanical and molecular simulation methods to investigate the formation energy, surface energy, polymorphic structure, lattice constants and the reaction path of the reactants and products in the electrolyte of a solid oxide fuel cell. These concepts were approached through possible presence of favored reaction sites in the structures of the geometries. We used the atomic simulation environment to make the models and we made calculations of the equations of state with density functional theory methods to obtain the most optimized geometries of the structures. Phase diagram calculations was included to describe the stable geometries from thermodynamic point of view. The barriers of dissociation was investigated with nudged elastic band method.

Chapter 1

INTRODUCTION

World has become strongly dependent on the excessive use of fossil fuels. And this has been utilized extensively to power automobiles, and factories, causing a dramatic build-up of greenhouse gases in the atmosphere. Unlike fossil fuels, the combustion of hydrogen does not generate carbon dioxide (CO_2) and carbonmono oxide (CO), but only water vapor and generating power with minimal greenhouse gases via fuel cells.
Threfore, a fuell cell needs materials to generate power like mostly used Pt but the cost of Pt is expensive when we compare to other materials such as Palladium, which is found abandantly in the earth covered 50% than Pt, and the palladiumum is an input to form Palladium Oxide with oxygen to be a material for fuel cell.

Fuel cells are widely considered to be a sustainable energy conversion system. Platinum is commonly used as anode and cathode catalyst in low temperature fuel cells. But the solid oxide fuel cell is a high temperature fuel cell and this palladium oxide compound is highly temperature resisitive compound up to 900°C. To reduce the cost of the fuel cells, one of the important challenges is the development of platinum-free catalysts or catalysts with a lower content of Pt. For all these reasons, binary and ternary platinum-based catalysts and non-platinum-based catalysts have been tested as electrode materials

for low temperature fuel cells. Therefore. palladium which has costs lower than those of platinum, and is at least fifty percent more abundant on Earth than Pt, can be substituted for Pt both as anode and cathode material without worsening fuel cell performance [1]. Palladium is thus studied for its functional properties to be as input in anode, cathode, or electrolyte form.

Noble-metal monoxide, specially PdO is compound of widespread technological interest for experimental chemistry and material science, as it possess unique catalytic properties (for example, as dehydrogenation catalysts) and other applications. Its functionality as a component of solid oxide fuel cell is investigated by applying density functional theory(DFT) method and various analysis tools such as nedged elastic band(NEB) and equation of states(eos) fits. From these, its bulk properties, stability, electronic structures and lattice constants are determined.

1.1 Fuel cells

A fuel cell is a device that uses hydrogen (or hydrogen-rich fuel) and oxygen to create electricity by an electrochemical process. A single fuel cell consists of an electrolyte sandwiched between two thin electrodes (a porous anode and cathode). Hydrogen, or a hydrogen-rich fuel, is fed to the anode where a catalyst separates hydrogen's negatively charged electrons from positively charged ions (protons).

At the cathode, oxygen combines with electrons and, in some cases, with species such as protons or water, resulting in water or hydroxide ions, respectively. The electrons from the anode side of the cell cannot pass through the membrane to the positively charged cathode; they must travel around it via an electrical circuit to reach the other side of the cell. This movement of electrons is an electrical current.

The amount of power produced by a fuel cell depends upon several factors, such as fuel cell type, cell size, the temperature at which it operates, and the pressure at which the gases are supplied to the cell. Still, a single fuel cell produces enough electricity for only the smallest applications. Therefore, individual fuel cells are typically combined in series into a fuel cell stack. A typical fuel cell stack may consist of hundreds of fuel cells. Fuel cells are classified primarily by the kind of electrolyte they employ. This determines the kind of chemical reactions that take place in the cell, the kind of catalysts required, the temperature range in which the cell operates, the fuel required, and other factors. There are several types of fuel cells currently under development, each with its own advantages, limitations, and potential applications.

1.2 Classification of Fuel Cells

Based on the type of Electrolyte

- Alkaline Fuel cell (AFC)
- Phosphoric Acid Fuel cell (PAFC)
- Polymer Electrolytic Membrane Fuel Cell (PEMFC)

  Solid Polymer Fuel Cell (SPFC) and

  Proton Exchange Membrane Fuel cell (PEMFC)
- Molten Carbonate Fuel Cell (MCFC)
- Solid Oxide Fuel Cell (SOFC)

1.3 Solid Oxide Fuel Cell, SOFC

Among the types of fuel cells we are focused on the Solid oxide fuel cell because now adays SOFC is in development than others and it is more environmental friendly fuel cell. Solid Oxide Fuel cells (SOFCs) have great potentials to produce clean energy in the form of electrical energy from chemical fuels with nearly zero pollutant emissions [2]. SOFCs also offer high levels of energy conversion efficiency [3] 60% - 70 % [4].

The SOFC electrolyte contains a dense solid metal oxide, which is how the name of this fuel cell was derived. Like all electrochemical cells, SOFC contain three basic components, a porous anode, an electrolyte membrane, and a porous cathode [5]. SOFCs utilize a yttrium stabilized zirconium (YSZ) electrolyte to transport oxygen ions between the cathode and anode. The electrolyte is also an electron insulator, forcing the electrons generated at the anode to flow through an external circuit, which can be used to satisfy a load. The oxidation reaction occurs at the anode, also known as the fuel electrode and the reduction reaction occurs at the cathode, also known as the air electrode [6].

1.3.1 Background on SOFCs

A SOFC is composed of three main components, the electrolyte and the two electrodes, i.e. anode and cathode. Fuel (e.g., hydrogen) is fed to the anode and is oxidized at the triple phase boundaries (TPB), formed by the electronic conducting, the ionic conducting and the gas phase. H_2 and oxygen ions from the electrolyte react to form water and electrons [7]:

$$H_2 + O^{2-} \rightarrow H_2O + 2e^- \tag{1.1}$$

Via an external circuit the electrons travel to the cathode, where the oxidant (e.g., oxygen) is electrochemically reduced:

$$\frac{1}{2}O_2 + 2e^- \rightarrow O2^- \tag{1.2}$$

The oxygen ions are conducted through the electrolyte to the anode to close the electrical circuit. Summing up Reactions (1.1) and (1.2) leads to the overall reaction:

$$H_2 + \frac{1}{2}O_2 \rightarrow H_2O \tag{1.3}$$

1.3.2 Components of SOFC

A single cell consists of three basic elements: electrolyte, anode and cathode. The cathode and anode electrodes are porous layered ceramic (cathode) and ceramicmetal (anode) components enabling easy gas diffusion to and from the electrode–electrolyte interfaces. They exhibit high electronic conduction and preferably also ionic conduction. The reduction and oxidation at the cathode and the anode respectively are spatially separated and the electrons are forced to flow through an external circuit. At the electrodes, the charge carrying species is changed from electrons from the outer circuit to the charged species the electrolyte can conduct. In the SOFC the electrolyte conducts O^{2-}-ions.

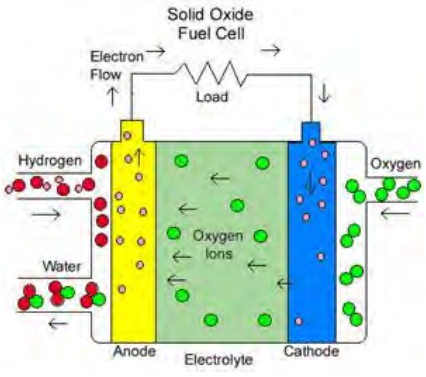

Figure 1.1: A Solid Oxide fuel cell [8].

The driving force for the migration of O^{2-} is the oxygen chemical potential gradient between the anode (low) and cathode (high). At the cathode, side air is usually used corresponding to an oxygen partial pressure (p_{O2}) of 0.21 atm. At the anode, the p_{O2} is very low due to the consumption of oxygen ions by the used fuel (in most cases hydrogen) to form water. The operating temperature of a SOFC is between 500°C and 1000°C because the conduction of oxygen ions in the solid electrolyte is a

thermally activated process. In contrast to other fuel cell types,a solid oxide fuel cell can be operated with a variety of fuels such as CH_4 with steam reforming and within a wide temperature range (500–1000°C). At the cathode, electrochemical reduction of oxygen occurs and the oxygen ions migrate through the electrolyte via a vacancy mechanism to the anode. At the anode, hydrogen is electrochemically oxidized to water [9].

- Anode Reaction: $2H_2 + 2O^{-2} \rightarrow 2H_2O + 4e^-$
- Cathode Reaction: $O_2 + 4e^- \rightarrow 2O^{-2}$
- Overall Cell Reaction: $2H_2 + O_2 \rightarrow 2H_2O$

1.4 Development of SOFCs

In 1992, a two-chamber solid electrolyte fuel cell was adapted to supply each electrode chamber with fuel-air mixtures. Cells were fabricated from Pt electrodes on an YSZ (yttria-stabilized zirconia) electrolyte and were operated at elevated temperatures in contrast to Dyer's room temperature device. Fuel cell operation was initialized either by an electrical pulse or different gas flow rates between the electrodes. For different electrode materials (e.g. Au and Pt), fuel cell operation was based on different electrochemical exchange rates of the two electrodes. Cell operation was possible using different fuels and at temperatures of up to 450 °C. At 350 °C for a methane-air mixture, an OCV of 0.95 V and a current of 0.065 mA at 0.64 V were measured. In another cell design, different gas flow rates were generated between the electrodes, enabling fuel cell operation without an initializing electrical pulse and up to 600 °C. Hibino and co-workers are the pioneers in implementing the single-chamber operating mode for high temperature SOFCs, making the use of hydrocarbon fuels possible and decreasing the risk of explosion as compared to H_2-O_2 mixtures. In 1993, Hibino et al. operated the first SC-SOFC in a methane-air

mixture at 950 C. In addition to the experimental demonstration of generating a significant current, outlet gas analysis and electrode potential measurements were used to elucidate the working mechanisms. The difference in catalytic activity of the electrodes for the partial oxidation of methane was found to lead to the generation of an OCV(open circuit voltage [7].

1.5 PdO

Palladium oxide, PdO, is a useful catalyst and is an ingredient in certain resistor-conductor compositions utilized by the electronics industry [10].

Palladium is a steel white, ductile and metallic element with its symbol Pd. In terms of earthly and cosmic abundance, it is one of the scarcest elements. Palladium was discovered in 1803 by the British chemist William H. Wollaston while he was purifying a quantity of crude platinum. It was named after the asteroid Pallas, which was discovered at about the same time [11].

1.5.1 Properties

The atomic number of palladium is 46, and its atomic weight is 106.42. Palladium's melting point is 1555 C (2831 F) and boiling point is 2963 C (5365 F). The malleable and ductile metal is harder than platinum. The specific gravity of the solid has been measured at 12.02, although the calculated density—based on the crystal lattice structure—yields a value of 12.0 g/cm3. Palladium is one of the six-member platinum family of precious metals (Group VIII). It is the least dense and lowest melting of the platinum family of elements. Palladium dissolves into acids more readily than any other platinum group member. The metal dissolves quickly in aqua regia, and it even dissolves, though slowly, in hydrochloric, nitric, or sulfuric acid. In finely divided form it is quite soluble in all acids. At room temperature it is not attacked by oxygen.

One of the unusual properties of the metal is that at room temperature it can absorb up to 900 times its own volume of hydrogen gas. When the metal is heated, hydrogen readily diffuses through it; this provides a means of purifying the gas [11].

PdO is stable in air up to 900^0C. Pd is therefore seldomly used as an electrode for electrochemical devices where a high exchange reaction kinetics is required at temperatures below 750^0C. High temperature fuel cells and oxygen pumps are, in contrast, often operated under conditions where Pd is stable.

1.5.2 Occurrence

Palladium is found along with the other metals of the group in platinum ores in deposits of the Russian Federation, South and North America, Ethiopia, and Australia. It is principally alloyed with gold and silver in a gold ore from Brazil. It also occurs with the nickel-copper deposits of South Africa and Ontario, Canada [11].

1.5.3 Compounds

The principal oxidation states of palladium are +2 and +4; valences of 0 and +1 are also exhibited, and a valence of +3 is rare. Three oxides can be formed with the metal. The best known, black palladium (II) oxide (PdO), is formed when the metal is heated in air at red heat. It is a strong oxidizing agent and is easily reduced to palladium metal by hydrogen gas. The monoxide is insoluble in water and acids, including aqua regia.
A brown hydrate of palladium (III) oxide (Pd2O3) is unstable and reverts to the monoxide in about four days. The compound loses water on heating and may explode as it changes to PdO. Palladium (IV) oxide (PdO2), the less common oxide, is formed as the hydrate, which has a dull red color [11].
It is well known that the effectiveness of palladium as oxidation catalysts depends strongly

on its complex reaction with gas-phase oxygen to form surface PdO [12].

Palladium oxide is the inorganic compound of formula PdO. It is the only well characterised oxide of palladium [13]. It is prepared by treating the metal with oxygen. It is not attacked by acids. Palladium oxide is prepared by heating palladium sponge metal in oxygen at 350°C [14].

- $2\text{Pd} + \text{O}_2 \rightarrow 2PdO$

1.5.4 Uses

Palladium is used mainly as a catalyst. Like other platinum metals, it exhibits catalytic activity in various reactions. Finely divided palladium is utilized as a catalyst for hydrogenation and dehydrogenation reactions. With other platinum metals, palladium is used in the catalytic converters of automobiles [11].

1.5.5 Stability

The power is generated by the fuel cells through the electrochemical reaction between oxgen and hydrogen [15]. The catalyst used to speed up the reaction is done by different monooxides like PdO; and Palladium has the ability to absorb large volumetric quantities of hydrogen at room temperature and atmospheric pressure.

Palladium Oxide is a highly insoluble thermally stable Palladium source suitable for glass, optic and ceramic applications. Palladium oxide is a greenish black powder that is immune to acids but reverts to palladium metal above 900°C. Oxide compounds are not conductive to electricity. However, certain perovskite structured oxides are electronically conductive finding application in the cathode of solid oxide fuel cells and oxygen generation systems. They are compounds containing at least one oxygen anion and one metallic

cation. They are typically insoluble in aqueous solutions (water) and extremely stable making them useful in ceramic structures as simple as producing clay bowls to advanced electronics and in light weight structural components in aerospace and electrochemical applications such as fuel cells in which they exhibit ionic conductivity.

Surfaces of palladium are excellent catalysts for chemical reactions involving hydrogen and oxygen, such as the hydrogenation of unsaturated organic compounds. Under suitable conditions (80°C and 1 atmosphere), palladium absorbs more than 900 times its own volume of hydrogen; it expands and becomes harder, stronger, and less ductile in the process. The absorption also causes both the electrical conductivity and magnetic susceptibility to decrease. A metallic or alloy-like hydride is formed from which the hydrogen can be removed by increased temperature and reduced pressure. Because hydrogen passes rapidly through the metal at high temperatures, heated palladium tubes impervious to other gases function as semipermeable membranes and are used to pass hydrogen in and out of closed gas systems or for hydrogen purification [16].

1.5.6 Geometric bulk and surface structure

PdO undergoes a first-order transition at about 12 GPa. The new phase is tetragonal and of similar cell dimensions to the low-pressure phase. However, it is more compressible along c and much harder along a. The volume change is 1.7%. It is likely that the new phase has the rocksalt structure [17] unit cell contains two PdO units with Pd atoms at all corners and in the center, and oxygen atoms at (0, 0, 0), (0, 1/2, 1/2)respectively (1/2, 1/2, 1/2), (1/2, 0, 0) , tetragonally elongated due to the low-spin d^8 electron configuration of palladium (II). The zero-pressure cell parameters and bulk moduli are (low pressure phase) a =3.042Å, c = 5.351Å, E =280 ± 52 GPa; (high pressure phase) a =2.982 Å, c = 5. 383 Å, E = 545 ± 20 GPa. One sample prepared was found to be a mixture of PdO with a cubic material [Fm 3m, a =4.043Åat ambient] [17].

PdO crystallizes in a tetragonal structure within theD_{4h}^{9} space group. There are two formula units of PdO in the tetragonal unit cell with Pd atoms at all corners and in the centre, and O atoms at (0, 1/2, 1/4), (0, 1/2, 3/4), (1, 1/2, 1/4) and (1, 1/2, 3/4) respectively. All Pd and O atoms are equivalent, with each Pd atom planar coordinated by 4 oxygen atoms, and each O atom tetrahedrally surrounded by 4 Pd atoms [18]. Using the method DFT-GGA approach the optimized lattice constants of the PdO unit cell are obtained as a = 3.051 Åand c = 5.495 Å. The Pd atom is coordinated by four planar oxygen atoms (fig.3.5) with a distance of 2.02Å. PtS type of structure (B17) at ambient conditions [19]. The geometrical structure of a unit cell for B17. The tetragonal unit cell contains two PdO units with Pd atoms at the center, and oxygen atoms at (0,1/2,1/2), (1/2,0,0) respectively (0,0,1/4), (0,0,3/4). The lattice constants are a=3.040Åand c=5.340 [20].

Chapter 2

METHOD

In this work, polymorphic models of the structures of PdO is considered. We used a relevant quantum mechanical and molecular simulation methods to investigate the kinetics of formations and barriers of dissociation of the reactants and products in the electrolyte of a solid oxide fuel cell. These concepts were approached through adsorptive reactions and possible presence of favored reaction sites in the structures of the geometries. The present calculations were calculated by means of Density Functional Theory method implemented in Abinit code. The exchange and correlation effect is treated with generalized gradient approximation (PBE) using the Perdew, Burke and Eruzeroff. The pseudopotentials were used with the condition pps = fhi, the energy cut = 400eV and the k-points sampling from $2 \times 2 \times 1$ to $16 \times 16 \times 16$ k – points were used to minimize the total energy. The self-consistent calculations were considered when the difference in the total energy of the crystal did not exceed 10^{-2}eV as calculated at consecutive steps. During this process, the structure is fully relaxed until the forces on the atom become smaller. For a small unit cell periodic system calculation, it is necessary to include k-points besides the Gamma point (sometimes the Gamma point is not even included in the calculation). This is because, what you should really calculate is a much bigger cell, which contains many unit cells. One Gamma point in the bigger cell corresponds to (folded back to)

many k-points in the Brilliouin zone of the (smaller) unit cell [21].

The k-point sampling from the point of Bloch's theorem, which allows one to only consider the electrons within the unit cell at an infinite number of k-points within the first Brillouin zone. As alluded to, it is possible to use only a finite number of k-points if these are chosen so as to appropriately sample the reciprocal space. One can therefore write an integrated function $f(\mathbf{r})$ over the Brillouin zone as

$$f(\mathbf{r})=\frac{\Omega}{(2\pi)^3}\int_{BZ} F(k)\mathrm{d}k = \sum_j \omega_j F(k_j) \tag{2.1}$$

where $F(\mathbf{k})$ is the Fourier transform of $f(\mathbf{r})$, Ω is the cell volume and the w_j are weighting factors. The set of "special" k-points chosen to appropriately sample the Brillouin zone is obtained in this work using the Monkhorst-Pack method. The k-points are distributed uniformly through space as

$$\mathbf{k}_j = x_{1j}\mathbf{b}_1 + x_{2j}\mathbf{b}_2 + x_{3j}\mathbf{b}_3 \tag{2.2}$$

where the $\mathbf{b}_i$ are reciprocal lattice vectors, and

$$x_{ij} = \frac{l_i}{n_j}, j = 1, \ldots, n_j \tag{2.3}$$

where the l_i are lengths of reciprocal lattice vectors, and n_j is an integer determining the number of special points in the set.

In practice, a further computational saving may be made by utilizing the point group symmetry of the lattice. This allows one to write the sums as

$$f(\mathbf{r}) = \sum_{j=1}^{P(n_j)} w_j F(\mathbf{k}_j) \tag{2.4}$$

where $P(n_j)$ is the symmetry-dependent number of points in the irreducible wedge

of the Brillouin zone. The weights in this equation are in general different to those in equation 2.1; they are simply the ratio of the order of the point group to that of the group of the wavevector $\mathbf{k}_j$ under consideration.

The number of k-points necessary for a calculation depends critically on the necessary precision and on the fact whether the system is metallic or nonmetallic. Metallic systems require an order of magnitude more k-points than semiconducting and insulating systems. The number of k-points also depends on the smearing method in use; not all methods converge with similar speed. In addition the error is not transferable at all i.e. a $9 \times 9 \times 9$ leads to a completely different error for fcc, bcc and sc. Therefore absolute convergence with respect to the number of k-points is necessary. The only exception are commensurable super cells. If it is possible to use the same super cell for two calculations it is definitely a good idea to use the same k-point set for both calculations.
It is recommended to use even meshes (e.g. $8 \times 8 \times 8$) for up to $n = 8$. From there on odd meshes are more efficient (e.g. $11 \times 11 \times 11$). However we have already stressed that the number of divisions is often totally unrelated to the total number of k-points and to the precision of the grid. Therefore a $8 \times 8 \times 8$ might be more accurate then a $9 \times 9 \times 9$ grid. For fcc a $8 \times 8 \times 8$ grid is approximately as precise as a $8 \times 8 \times 8$ mesh [22].

2.1 Density Functional Theory, DFT

The execution of many atomic-scale simulations requires information about energies and forces of atoms, and these can be calculated by several methods. One of the most popular approaches is density functional theory (DFT) which is implemented in different ways in dozens of freely available codes [**?**].
DFT codes calculate atomic energies and forces by solving a set of eigenvalue equations describing the system of electrons. A simpler but also more approximate approach is to

use interatomic potentials (or so-called force fields) to calculate the forces directly from the atomic positions [23]. The Coulomb interaction potential between an electron and the rest of the electrons is approximated by a mean field potential, V_H ,[24] written as

$$V_H(r) = \int \frac{n(r')}{|r - r'|} d^3r' \tag{2.5}$$

Where $n(r')$ is electron density with the ground state density of nucleus given by :

$$n(\mathbf{r}) = \sum_{\mathbf{i=1}}^{\mathbf{N}} \mid \psi_{\mathbf{i}}(\mathbf{r}) \mid^{\mathbf{2}} \tag{2.6}$$

The Hamiltonian operator corresponding to each electron is thus,[24]

$$\hat{H} = \hat{T} + \hat{V} + \hat{V}_H$$

where $\hat{V}$ is the interaction term between an electron and the nuclei, $\hat{T}$ is the Kinetic energy and $\hat{V}_H$ is the mean field potential.

From the Schrödinger equation:

$$\hat{H}\psi(\mathbf{r}) = E\psi(\mathbf{r}) \tag{2.7}$$

where H is an operator, H=H[$n(\mathbf{r})$],and E is the energy of the system, E=E[$n(\mathbf{r})$].

The Kohn-Sham(KS) Theory, which is considered the electronic energy of a molecule:

$$E = T + V_{ne} + V_{ee} + V_{xc} \tag{2.8}$$

Where T is Noninteracting kinetic energy, V_{ne} is Coulomb interaction with nuclei, V_{ee} is

Coulomb interaction of electron density n(r) with itself and V_{xc} is exchange-correlation energy. Hence, written in Schrödinger equation form:

$$H_{KS}\psi(\mathbf{r}) = \mathbf{E_{KS}}\psi(\mathbf{r}) \tag{2.9}$$

where H_{KS}=$H_{KS}[n(\mathbf{r})]$, E_{KS}=$E_{KS}[n(\mathbf{r})]$.

Here,

$$n(\mathbf{r}) = \sum\nolimits_{\mathbf{i=1}}^{\mathbf{N}} \mid \psi_{\mathbf{i}}(\mathbf{r}) \mid^{\mathbf{2}} \tag{2.10}$$

2.1.1 Exchange-correlation energy functionals

Local density Approximation, LDA

The simplest approximation for the exchange-correlation energy function, is the local-density approximation (LDA). The exchange-correlation energy of the homogeneous electron gas, i.e., a system with a constant electron density is known.

In LDA this exchange-correlation energy for the homogeneous electron gas is also used for non-homogeneous situations. In other words, the exchange-correlation energy of an inhomogeneous system can be obtained by using the density of the homogeneous electron gas to approximate the inhomogeneous density in any point locally.

In practice, total energy calculations require approximat ions to be made for the exchange-correlation energy, E_{xc} and Kohn and Sham showed that the local density (LD) approximation [25],

$$E_{x_c}^{LDA}[n] = \int n\,(r)\,\epsilon_{x_c}^{LDA}(n\,(r))\,\mathrm{d}r. \tag{2.11}$$

Where $E_{x_c}^{LDA}$ is Exchange-correlation energy of local density approximation, n(r) is electron density and $\epsilon_{x_c}^{LDA}$ is energy density.

The local density approximation, LDA is a good approximation for systems with slowly varying electron density, but for strongly inhomogeneous systems like, e.g. atoms or molecules, or reactions at surfaces, LDA results may not be sufficiently accurate. Usually LDA shows over-binding, i.e. binding and cohesive energy turn out to be too large compared to experiment. This over-binding also leads to lattice constants and bond lengths that are smaller compared to the experimental values [26].

Bulk structural properties are often not improved within the generalized gradient approximation, GGA. While the lattice parameters consistently increase compared to the LDA [27] The generalized gradient approximation improves on the LDA by including the gradient of the density, (r), to account approximately for the non-homogeneity of the true electron density [28]. The exchange functional is:

$$E_{x_c}^{GGA}[n] = \int n\,(r)\,\epsilon_{x_c}^{GGA}(n\,(r)\,, \nabla n(r))\,\mathrm{d}r. \tag{2.12}$$

Where $E_{x_c}^{GGA}$ is Exchange-correlation energy of generalized gradient approximation, n(r) is electron density and $\epsilon_{x_c}^{GGA}$ is energy density

in which also a gradient of the density is included in the exchange-correlation energy [26].

2.2 Birc-Murnghan fit Methods

The Equation of State is a pressure-volume or energy-volume relation describing the behavior of a solid under compression or expansion. The simplest isothermal equation of state(eos) for a solid is the bulk modulus which is a measure of the ability of a material in resisting to changes in volume under uniform compression or expansion.

The equilibrium bulk modulus B_0 of a crystal can be defined as follows:

$$B_0 = -V\left(\frac{\partial P}{\partial V}\right)_T \tag{2.13}$$

A dimensionless parameter B_0 can then be defined as its first derivative with respect to the pressure, at constant temperature T:

$$B_0^{'} = \left(\frac{\partial B_0}{\partial V}\right)_T \tag{2.14}$$

Let us recall that the pressure P may be written as a function of the volume V as:

$$P(V) = -\left(\frac{\partial E}{\partial V}\right)_S \tag{2.15}$$

According to equation (2.14) we can redefine the bulk modulus in equation (2.12) as the second energy derivative with respect to the volume:

$$B(V) = V\left(\frac{\partial^2 E}{\partial V^2}\right)_{T,S} \tag{2.16}$$

We can now define the enthalpy H (coinciding with Gibbs' free energy G at T=0 K, the standard temperature of abinit calculations) as a function of the volume V simply as:

$$H(V) = E(V) + P(V) \times V \tag{2.17}$$

Thus,in 1944, Murnaghan proposed his famous equation of state which is based on the assumption that the bulk modulus varies linearly with pressure:

$$E(V) = E_0 + \frac{B_0 V}{B_0^{'}}\left[\left(\frac{V_0}{V}\right)^{B_0^{'}} \frac{1}{B_0^{'}-1} + 1\right] - \frac{B_0 V_0}{B_0^{'}-1} \tag{2.18}$$

where V_0 and E_0 are the equilibrium volume and energy, at zero pressure. Application

of equation (2.14) to equation (2.17), gives P(V) Murnaghan's EOS:

$$P(V) = \frac{B_0 V}{B_0'}\left[\left(\frac{V_0}{V}\right)^{B_0'} - 1\right] \tag{2.19}$$

Then the third-order Birch-Murnaghan isothermal equation of state (based on the Eulerian strain), published in 1947, reads like:

$$E(V) = E_0 + \tfrac{9V_0B_0}{16}\left\{\left[\left(\tfrac{V_0}{V}\right)^{2/3} - 1\right]^3 B_0' + \left[\left(\tfrac{V_0}{V}\right)^{2/3} - 1\right]^2 \left[6 - 4\left(\tfrac{V_0}{V}\right)^{2/3}\right]\right\} \tag{2.20}$$

2.3 Abinit

In order to set up the atomic structure, one has to define the unit cell (unit cell of the crystal or supercell for a molecule), the atom types, and the atomic positions using ABINIT [29]. And ABINIT is a package whose main program allows one to find the total energy, charge density and electronic structure of systems made of electrons and nuclei (molecules and periodic solids) within Density Functional Theory (DFT), using pseudopotentials and a planewave basis. ABINIT also includes options to optimise the geometry according to the DFT forces and stresses, or to perform molecular dynamics simulation using these forces, or to generate dynamical matrices, Born effective charges, and dielectric tensors. Excited states can be computed within the Time-Dependent Density Functional Theory (for molecules, or within Many-Body Perturbation Theory (the GW approximation) [30].

2.4 ASE

We used the atomic simulation environment to make the models and we made calculations of the equations of state with density functional theory methods to obtain the most optimized geometries of the structures. And the Atomic Simulation Environment (ASE) is a collection of Python modules intended to set up, control, visualise, and analyse simulations at the atomic and electronic scales. ASE provides Python classes like "Atoms" which store information about the properties and positions of individual atoms. In this way, ASE works as a front-end for atomistic simulations where atomic structures and parameters controlling simulations can be easily defined [31].

2.5 Nudged elastic band, NEB

The Nudged Elastic Band (NEB) method is a technique for finding transition paths (and the corresponding energy barriers) between given initial and final states of a chemical reaction. The method works by first constructing a chain of replicas or images of the system. The chain is then deformed in order to minimize the energy barrier for the reaction.

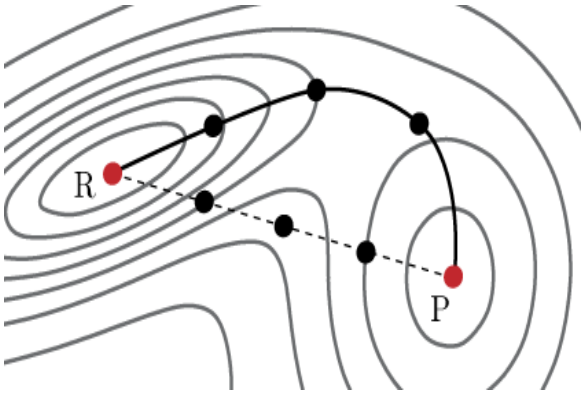

Figure 2.1: Nudged Elastic Band method: To determine the energetic minimum path between the reactant and product state of a chemical reaction.[32] *Reaction path optimization using the Nudged Elastic Band method*

An initial band (dashed) is constructed connecting the positional configuration of the two states (red circles). A sequence of linear interpolated images (black circles) are then positioned equidistantly along the band (black circles).

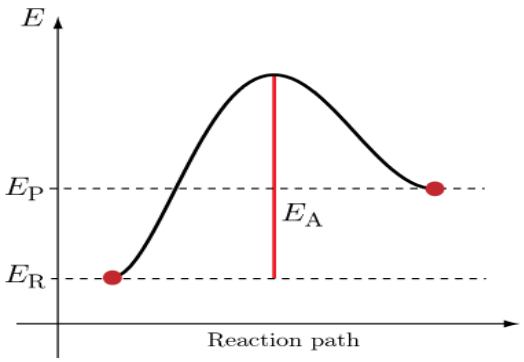

Figure 2.2: A typical energy variation between the reactant and product states of a chemical reaction. The figure describes the energy variation along the minimum path shown in Figure 2.1 with a solid line. In order for the reaction to occur, an energy threshold (red vertical line), the so-called activation energy EA, must be overcome.
[32]

The location of the band is then minimized through a series of iterations yielding a minimum embedding of the band on the potential energy surface (solid line). A typical variation of the energy along the minimized band path is displayed in Figure 2.2.

2.6 Crystal structure and computational details

The energy calculations presented in this paper are performed within the framework of the density functional theory (DFT), using the ABINIT. The PBE generalized gradient approximation (GGA) is applied for the exchange–correlation functional and the pseudopotentials method for determining activation energies, reaction pathways are obtained by means of the nudged elastic band (NEB) method as implemented in ABINIT. The

periodically repeated simulation cell includes a slab of four and a vacuum gap between the slabs larger than 10 Å as shown in the figure(Fig.3.12 - 3.14). All simulations are performed within the (2×2) surface unit cell of PdO(1 0 0). The wave functions are expanded in plane waves up to a kinetic energy cut-off of 400 eV. Integration in the first Brillouin zone is performed using Monkhorst–Pack grids including $6 \times 6\hat{A}$ 1 k-points. All calculations are performed without zero-point energy correction. Molecules are adsorbed only on one side of the slab. The adsorbed molecules and the two outer atomic layers of the slab are allowed to relax, whereas the atom positions in the remaining two layers of the slab are kept fixed. The isolated species in the vacuum (O_2, H_2, . . .) have been calculated in the same cell as the slab, with the same computational parameters.

2.7 Surface energy

Surface energy, or interface energy, quantifies the disruption of intermolecular bonds that occur when a surface is created. In the physics of solids, surfaces must be intrinsically less energetically favorable than the bulk of a material (the molecules on the surface have more energy compared with the molecules in the bulk of the material), otherwise there would be a driving force for surfaces to be created, removing the bulk of the material (see sublimation). The surface energy may therefore be defined as the excess energy at the surface of a material compared to the bulk, or it is the work required to build an area of a particular surface. Another way to view the surface energy is to relate it to the work required to cut a bulk sample, creating two surfaces.

Cutting a solid body into pieces disrupts its bonds, and therefore consumes energy. If the cutting is done reversibly (see reversible), then conservation of energy means that the energy consumed by the cutting process will be equal to the energy inherent in the two new surfaces created. The unit surface energy of a material would therefore be half of its energy of cohesion, all other things being equal; in practice, this is true only for

a surface freshly prepared in vacuum. Surfaces often change their form away from the simple "cleaved bond" model just implied above. They are found to be highly dynamic regions, which readily rearrange or react, so that energy is often reduced by such processes as passivation or adsorption [33].

Converged values for the sensitive surface properties reported in Table 3.2 are obtained based on four layer (11) slabs of the Pd(111), Pd(100), and Pd(110) unit cells (i.e. one atom per layer), and a vacuum distance of 10 Å. We employ a sufficiently dense ($6 \times 6 \times 1$) Monkhorst-Pack sampling grid with a similar quality($6 \times 6 \times 6$) mesh for the bulk energy, as discussed by Da Silva et al. Upon increasing the slab thickness to seven layers, we find minimal changes to the computed surface energies on the mJ/m 2 scale (specifically, 6 mJ/m^2 for Pd(111), 15 mJ/m^2 for Pd(100), and 24 mJ/m^2 for Pd(110)). Qualitative trends in surface relaxations remain unaltered within slabs of a five- to eight-layer thickness. However, for reasons of consistently comparing to the values of Table 3.2, we note that all values on interlayer spacings that are reported in the following (i.e. also upon O adsorption) are given based on eight-layer slab calculations. Relaxations are conducted using the Broyden-Fletcher-Goldfarb-Shanno (BFGS) algorithm with a force convergence criterion of F max 10^3 eV/Å, while all layers in the slab are allowed to relax [33]. Finally, we note that surface energies are calculated according to the commonly employed strategy:

$$\sigma = \frac{1}{2A}\left(E_{slab} - \frac{N_{slab}}{N_{bulk}}E_{bulk}\right) \tag{2.21}$$

where E_{slab} , E_{bulk} are the total energies from comparable slab and bulk calculations and E_{slab} , E_{bulk} are the number of atoms in the two respective model structures. The factor of 1/2 accounts for the fact that the surfaces come in pairs in the symmetric slab calculations, while A is the specific surface area of the employed slab model.

Chapter 3

RESULTS AND DISCUSSIONS

3.1 The Geometric bulk and surface structure

The calculations were carried out for three types of theoretically reported polymorph, i.e., rock-salt type (B1), tetragonally elongated rock-salt (t-B1), and the PtS type or B17 type of PdO.

Palladium oxide crystallizes in B1, t-B1, and the tetragonal PtS-structures with space group D_{4h}. Each Pd atom of PdO in rocksalt structure is planar coordinated by four oxygen atoms and each O atom is surrounded by six Pd atoms see Fig. 3.1. For Pd atom of PdO in t-B1 structure is planar coordinated by two oxygen atoms and each atom is surrounded by three Pd atoms. The tetragonal unit cell contains two PdO units with Pd atoms at all corners and in the body center, and oxygen atoms at (0,0,0), (1/2,1/2,1/2) and oxygen atoms at (0,1/2,1/4), (0,1/2,3/4), see Fig. 3.2. The B17 structure of PdO type of Pd is planar coordinated by four oxygen atoms and each Pd atom is surrounded by four oxygen atoms. The tetragonal unit cell contains two PdO units with Pd atoms at (0,1/2,1/2), (1/2,0,0) and oxygen atom at (0,0,1/4), (0,0,3/4), see Fig. 3.3

Also for the palladium oxide the lattice constants are optimized individually for GGA exchange-correlation functional. The calculated lattice constants of rocksalt, t-B1, and

B17 at room temperature are a = 4.550 Å and c = 4.550 Å (c/a = 1), a = 3.096 Å and c = 5.454 Å (c/a = 1.762), and a = 3.116 Å and c = 5.425 Å(c/a = 1.741), respectively. The calculated values are presented in Tab. 3.1.

Table 3.1: DFT Parameters:Computed structual parameter of PdO compared with different functionals and experimental results.

PdO	**a**(Å)	**c**(Å)	**Bulk**(GPa)	**E/atom**(eV)	$\mathbf{E}_{tot}$(eV)	$\triangle H_f$(eV)	**Cor.no**
Our Rock-salt	4.550	4.550	177.638	-7.110	-28.438	15.468	6
Expermental[17]	4.043	4.043	-	-	-		-
Our BC-Tetra	3.096	5.454	261.078	-16.005	-64.020	-9.062	5
Expermental[34]	3.043	5.336	-	-	-	-	-
Theotetical(DFT)[35]	3.051	5.495	-	-	-	-	-
Our FC-Tetra(B17)	3.116	5.425	270.959	-16.025	64.102	-9.226	4
Expermental[20]	3.040	5.340	-	-	-	-	-

The optimized structural parameters, namely lattice constant parameter and compared previously reported value of energy from density functional theory as shown in Table 1 and bond length between Pd and O are 2.08 Å. The calculated lattice parameter is in good agreement with the previously reported values as shown in Table 3.1

Stoichiometric PdO has cubic and tetragonal perovskite structure at room temperature with D_{4h} space group. The structural phase transition from cubic to tetragonal occurs at higher temperature.As shown Fig. 3.1, the structure contains 13-coordinated Palladium ions occupying 8 at corner positions and 5 at face center , whereas the oxygen contains 12-coordinated ions at the center of the cubic cell, is surrounded by 4 palladium ions.

And PdO has also two additional types of structures as show in Fig. 3.2 and Fig.3.3 which are tetragonal type t-B1 and B17. The structure of tetragonal t-B1 contains 12-coordinated Palladium ions occupying 8 at corner positions and 1 at body center surrounded by four oxygen. The other tetragonal type structure known as B17 type structure or PtS structure type, which contains 6-coordinated Palladium ions occupying 4 at the center of the cubic cell and 2 palladium ions occupying at the face of the cubic

cell surrounded by four oxygen ions for each.

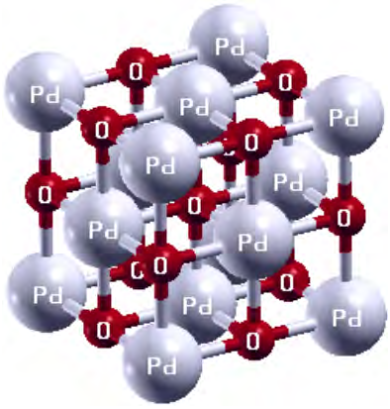

Figure 3.1: Rocksalt unit cell of PdO(Small red spheres indicate oxygen atoms, large white ones Pd atoms.)

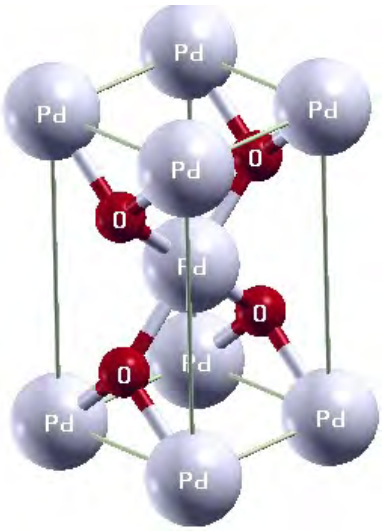

Figure 3.2: Body-centered unit cell of PdO(The tetragonal bulk unit cell of PdO. Small red spheres indicate oxygen atoms, large white ones Pd atoms.)

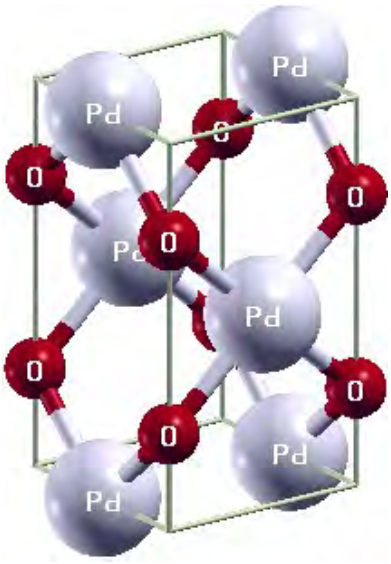

Figure 3.3: B17-type cell of PdO(The tetragonal bulk unit cell of PdO. Small red spheres indicate oxygen atoms, large white ones Pd atoms.)

PdO is indeed a semiconductor in confirmation of the work on polycrystalline films of Okamoto and Aso (I), that the oxide as normally obtained from reagent-grade chemicals is heavily doped with active acceptor levels at energies from 0.0 to 0.1 eV above the highest filled band, and that these acceptors give rise to extrinsic p-type conductivity.[10] the Fermi level would be expected to lie in an energy gap consistent with the observed semiconductivity[10] of PdO.

The general approach is illustrated by the example in Figure (3.4 - 3.5), which shows the total energy as a function of the lattice parameter a for the PdO.

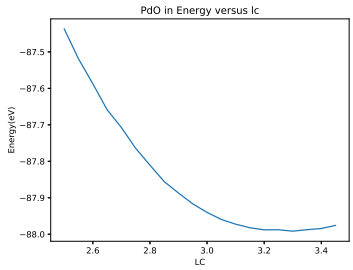

Figure 3.4: The total energy per unit cell as a function of the lattice parameter a for the PdO t-B1 type used for the values in Table 1.

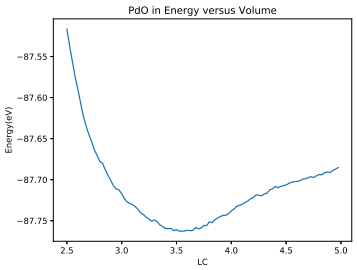

Figure 3.5: The total energy per unit cell as a function of the lattice parameter a for the PdO B17 type used for the values in Table 1.

From Fig. 3.4 and Fig. 3.5 the lattice constants found for each polymorphic structure of PdO at the lowest energy level where the graph converged. The energy versus volume graph of the three polymorphic structure of PdO are shown in Fig.3.6, 3.7 and 3.8. From the volume at the lowest point in the graph, the lattice constant is determined.

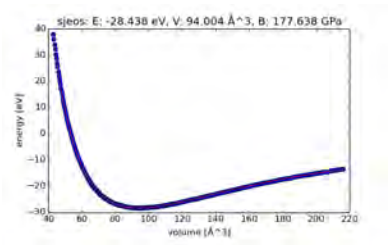

Figure 3.6: PdO-rocksalt-energy-versus-volume.

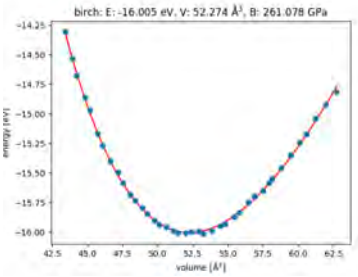

Figure 3.7: PdO-tetra B1-energy-versus-volume.

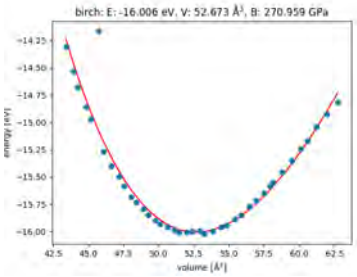

Figure 3.8: PdO-tetra B17-energy-versus-volume.

3.2 Surface Structures and relative stabilities

The most favorable PdO surfaces under particular conditions are calculated and tabulated (listed in Table 3). Among all structures, higher coverage adlayers with strong oxygen adsorption energies are found to be most favorable. These involve substantial roughening of the first atomic metal layers. On the PdO(100) surface(see Fig. 3.9). In the unit cell of this structure two O atoms prefer being located below and two atoms above the first Pd layer, so as to form an O–Pd–O four layer. Despite the structural similarity, the electronic properties of these surfaces are different. On the PdO(111) surface, the most stable structure among all the coverages that we investigated for PdO(111) involves a $\sqrt{6} \times \sqrt{\times}$ 6 arrangement of O atoms with the Pd_4 O_5 stoichiometry (Fig. 3.10). Also in this unit cell, there is a strong surface reconstruction, and four O atoms coordinate in plane to the surface Pd atoms. On the PdO(110) surface, adlayers with higher oxygen surface coverages are the more stable ones as shown in (Fig. 3.10), but they are only loosely related to the bulk PdO structure. And that PdO(111) is the most stable surface.

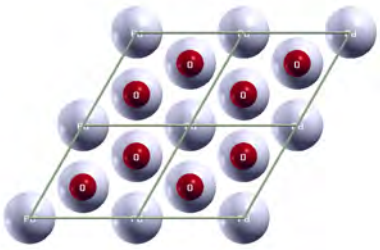

Figure 3.9: stoichiometry of surface PdO(100) 2×2

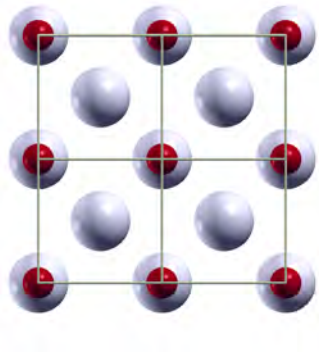

Figure 3.10: stoichiometry of surface PdO(110)2×2

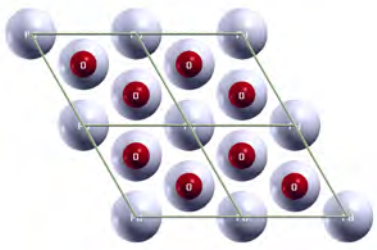

Figure 3.11: stoichiometry of surface PdO(111)2×2

Under these conditions the preferred shape of the PdO is a polyhedron consisting mainly of (111) and (100) facets. The evaluation of the surface energy is summarized in the spreadsheet below. Due to the choice of a primitive cell for the bulk PdO calculation,

a k-mesh of $6 \times 6 \times 1$ corresponds most closely to the $6 \times 6 \times 1$ k-mesh used in the slab calculations. The effect of different separation (thickness of vacuum) is tested here by calculating the total energy of a 4-layer slab model with a c-parameter of 10 Å. The surface energy is computed from energies Abinit calculation by subtracting n-times the bulk reference for PdO (primitive cell), and dividing through the surface area.

Table 3.2: Computed structual parameter and electronic band gaps of PdO compared with different functionals and experimental results.

Surface	$\mathbf{E}_{ads}$(eV)
PdO(100)	-1.71
Theoretical[33]	-1.58
PdO(110)	-1.69
Theoretical[33]	-1.58
PdO(111)	-1.53
Theoretical[33]	-1.49

The three surface energies calculated and the referenced values are nearly close as shown in Table 3.2.

3.3 Electronic properties:

The density of states (DOS) is essentially the number of different states at a particular energy level that electrons are allowed to occupy, i.e. the number of electron states per unit volume per unit energy. Bulk properties such as specific heat, paramagnetic susceptibility, and other transport phenomena of conductive solids depend on this function. DOS calculations allow one to determine the general distribution of states as a function of energy and can also determine the spacing between energy bands in semiconductors[36].Based on this the calculated electronic band structure total density of states using PBE functional is shown in Fig 3.15, The band gap energy of 1.3eV compare well with the experimental value of 1.5eV and other obtained value. PdO is asemiconductor with a small direct band gap at the M-point of the Brillouin zone(BZ). The PdO band gap are not consistent but vary in the range 0-2.67 eV.

3.4 Reaction path of H_2, O_2 and H_2O

The reaction path of Fig.3.12 and Fig.3.13 show that the oxygen and Hydrogen molecules reactions on the surface of PdO with large activation energy, and tha is endothermic type while the Fig. 3.14 the the water byproduct shows that the exothermic type.

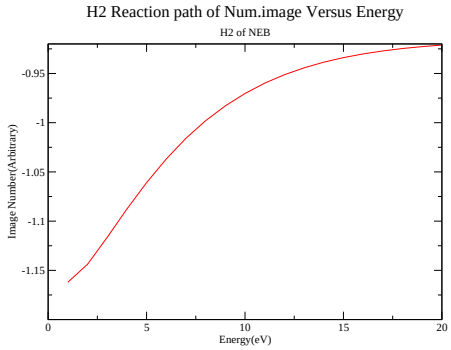

Figure 3.12: H_2-reaction path energy.

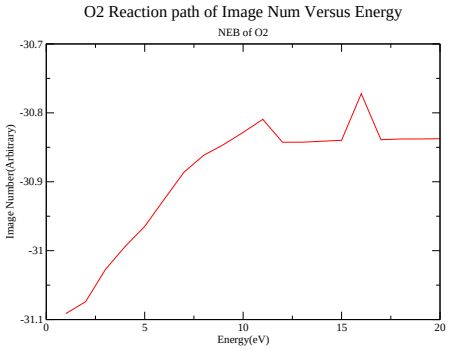

Figure 3.13: O_2 reaction path-energy.

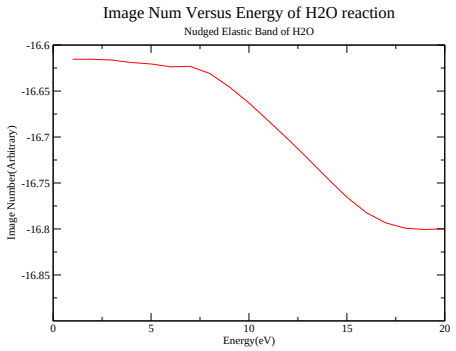

Figure 3.14: H_2O reaction path-energy.

3.5 Density of state

Density of states (DOS) is a description of the number of electronic states at each energy level available to be occupied by electrons. High density at specific energy levels translates to the availability of many states for occupation while a DOS of zero indicates that no states can be occupied at that energy level. DOS analysis provides an insight into the

electronic band structure of a system and helps identify valence and conduction bands, band gaps and Fermi-level of a system. Valence band is the highest range of electron energies in which electrons are present when the system is at absolute zero temperature [37]. Valence band is located below the conduction band which is the range of electron energies enough to free an electron from its binding with an atom and move freely within the atomic lattice of the material as a delocalized electron. Separation between valence and conduction band is referred to as the band gap and no electron states exist in this region. The Fermi-level is a hypothetical energy level that represents the total chemical potential for electrons in a system. Thus, the total density of states of PdO is plotted at abinit condition and is shown below in the Fig 3.10, 3.11 and 3.12.

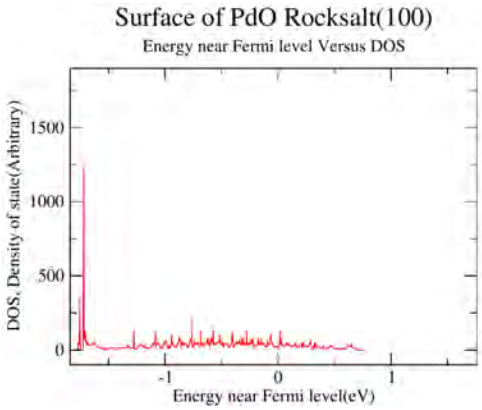

Figure 3.15: Calculated density of states (DOS) of PdO in rocsalt type within the conventional PBE method.

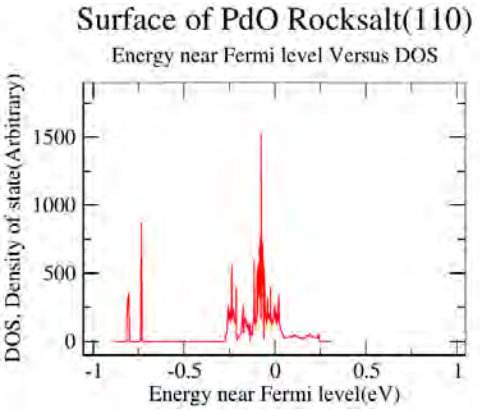

Figure 3.16: Calculated density of states (DOS) of PdO in tetragonal t-B1 type within the conventional PBE method.

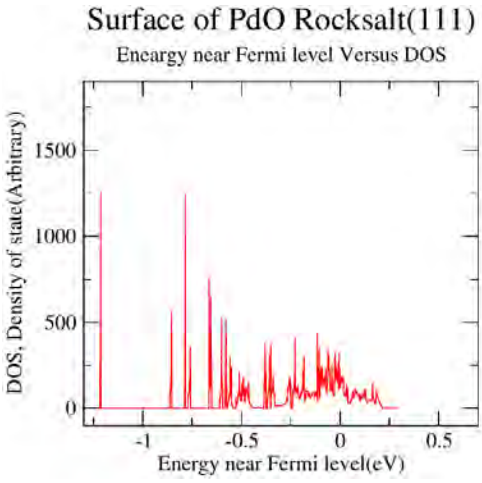

Figure 3.17: Calculated density of states (DOS) of PdO in rocsalt type within the conventional PBE method.

Chapter 4

CONCLUSION

This work has centered on the functional properties of PdO treating as a component of fuel cell using the method DFT calculations. We outlined the basic theory of Kohn-Sham DFT as a means of effectively solving the many-electron Schrödinger equation that describes most of the physics of condensed matter. We then described how this theory can be implemented with Abinit pseudopotentials approach, using as an example the ABINIT code, which we have used for all the calculations in this work.

In this paper also we have studied the structural and electronic properties of PdO under abinit condition by using the DFT method implemented in Abinit code. Equilibrium lattice parameter of this compound is calculated. The DOS diagram indicates the covalent bond between Pd and O. The band structure shows the insulator nature of this compound.When an atom (or molecule) is adsorbed on a surface, it usually favours a given high symmetry site. Such a preference is identified by comparing the energetics of different geometries with the adsorbate in varying sites. The structure with the lowest energy is then the most stable one, within the subset of considered adsorbate phases at a certain coverage.

Bibliography

[1] *Ermete Antolini, Palladium in fuel cell catalysis, Energy Environmental Science, 7th May 2009*

[2] *Shahriar Bozorgmehri , Mohsen Hamedi , and Alireza Babaei ,Modeling of Nanostructured Palladium Anode in Solid Oxide Fuel Cells, © (2014) Trans Tech Publications, Switzerland Vol. 829 (2014) pp 195-198*

[3] *J.Larminie and A. Dicks, Second Edition, Fuel Cell Systems Explained, ohn Wiley Sons Ltd, The Atrium, Southern Gate, Chichester,*

[4] *D. M. Bastidas, High temperature corrosion of metallic interconnects in solid oxide fuel cells, CENIM-National Centre for Metallurgical Research, 9 de octubre de 2006.*

[5] *Allan J. Jacobson, Materials for Solid Oxide Fuel Cells, American Chemical Society, October 9, 2009*

[6] *Hasson, Ian, "An Investigation of Two Ceramic Electron Conductors for Use in Solid Oxide Fuel Cell Anodes" (2011). Master's Theses.Paper 22.*

[7] *Melanie.Kuhn-Teko W.Napporn, Single-Chamber Solid Oxide Fuel Cell Technology—From Its Origins to Today's State of the Art, Energies, 15 January 2010*

[8] *http://americanhistory.si.edu/fuelcells/index.htm, A Basic Overview of Fuel Cell Technology*

[9] *Ludwig.J.etal, Solid Oxide Fuel Cells:Systems and Materials, CHIMIA International Journal for Chemistry, Volume 58, Number 12, December 2004, pp. 837-850(14)*

[10] *D. B. Rogers, R. D. Shannon and J. L. Gillson, Crystal Growth and Semiconductivity of Palladium Oxide,Central Research Department, E. I. du Pont de Nemours and Company, November 20,197O*

[11] *Encyclopedia.America, Palladium*

[12] *Alireza Babaei , Lan Zhang , Erjia Liu , San Ping Jiang , Performance and stability of La 0.8 Sr 0.2 MnO 3 cathode promoted with palladium based catalysts in solid oxide fuel cells, Elsevier, 2011/4/7*

[13] *E.H. Voogt, A.J.M. Mens, O.L.J. Gijzeman , J.W. Geus, XPS analysis of palladium oxide layers and particles, Elsevier, 20 April 1996*

[14] *http://www.americanelements.com*

[15] *Selvaraj.V , Sivakumar.R and Raja Sekaran.G, Modeling and Simulation of Solid Oxide Fuel Cell System, International Journal of Innovative Science, Engineering Technology, Vol. 1 Issue 9, November 2014.*

[16] *Arezoo Dianat, Nicola Seriani , Lucio Colombi Ciacchi, Manfred Bobeth , Gianaurelio Cuniberti, DFT study of reaction processes of methane combustion on PdO(1 0 0), Chemical Physics 443 (2014) 53–60*

[17] *Andrew.G.Christy, Simon M. Clark, Structural behavior of palladium (II) oxide and a palladium sub-oxide at high pressure:An energy-dispersive x-ray-diffraction study, Daresbury Laboratory, 8'arrington WA44AD, England and Department of Chemistry, University of Leicester, Leicester LEl 7RH, England, VOLUME 52, NUMBER 13, 2 May 1994*

[18] *Seung-Hoon Oh, Gar B. Hoflund, Low-temperature catalytic carbon monoxide oxidation over hydrous and anhydrous palladium oxide powders, Elsevier, 1 January 2007*

[19] *Masato M OGI, Yasuhide I NOUE , Tomoyuki Y AMAMOTO , Isao T ANAKA , Ponnusamy N ACHIMUTHU and Rupert C. C. P ERERA, Near-edge X-ray Absorption Fine Structure of PdO at O K-edge, Japanese Journal of Applied Physics, Vol. 44, No. 6A, 2005, pp. 4057–4059*

[20] *N. Kasper, P. Nolte and A. Stierle, Stability of Surface and Bulk Oxides on Pd(111) Revisited by in Situ Xray Diffraction, pubs.acs.org/JPCC*

[21] *http://cmsn.lbl.gov/, Basic concepts for k-points and symmetry*

[22] *https://cms.mpi.univie.ac.at/, Number of k-points, and method for smearing*

[23] *https://openkim.org, Knowledgebase of interatomic models.*

[24] *Kenate Nemera Nigussa, Density Functional Theory Investigations of Surface Structure and Reactivity, NTNU Open, 2011*

[25] *R. O. Jones, Introduction to Density Functional Theory and Exchange-Correlation Energy Functionals, Computational Nanoscience: Do It Yourself!,J. Grotendorst, S. Bl ugel,D. Marx (Eds.),John von Neumann Institute for Computing, J ulich,NIC Series, Vol. 31, ISBN 3-00-017350-1, pp. 45-70, 2006.*

[26] *Mira.Todorova, Oxidation of Palladium Surfaces, Berlin 2004*

[27] *M. Fuchs, M. Bockstedte, E. Pehlke, and M. Scheffler, Pseudopotential study of binding properties of solids within generalized gradient approximations:The role of core-valence exchange correlation, Fritz-Haber-Institut der Max-Planck-Gesellschaft, Faradayweg 4-6, D-14195 Berlin-Dahlem, Germany, 11 July 1997*

[28] *Tianhou Zhang, Theoretical studies of fuel cell reaction mechanisms:H_2 and O_2 on platinum electrodes, Case Western Reserve University, August, 2008*

[29] *https://findwords.info/term/abinit, What is "abinit"*

[30] *http://www.psi-k.org/codes.shtml, Psi-k - Electronic Structure Calculation of Solids and Surfaces*

[31] *http://psi-k.net*

[32] *https://quantumwise.com/documents/manuals/ATK-2008.10/chap.relax.html, Reaction path optimization using the Nudged Elastic Band method*

[33] *Vanessa J.Bukas.Karsten Reuter, A comparative study of atomic oxygen adsorption at Pd surfaces from Density Functional Theory, Elsevier, April 2017*

[34] *Shivam.Kansara.etal, Density functional study of structural,electronic and vibrational properties of palladium oxide, Elsevier, November 2016*

[35] *Jutta Rogal, Karsten Reuter, and Matthias Scheffler, On the thermodynamic stability of PdO surfaces, Fritz-Haber-Institut der Max-Planck-Gesellschaft, Faradayweg 4-6, D-14195 Berlin, Germany, 27 February 2004*

[36] *http://electrons.wikidot.com/, Density of States - MSE 5317*

[37] *Abbin Antony, Afirst principle study of chemical activity on PdO(101) thin film surface, University of Florida 2013*

4.1 Declaration

I declare that the thesis hereby submitted to the Addis Ababa University (AAU) for the degree of Master of Science has not previously been submitted by me for a degree at this or any other university, that it is my own work both in design and execution, and that all material contained herein has been duly acknowledged.

Name: Mulugeta Aregay

Date , Signature

Place and time of submission: Addis Ababa University, June 2017

This Thesis has been submitted for examination with our approval as University advisor.

Name: Dr.Kenate Nenera

Date , Signature

Name: Dr.Lemi Demeyu

Date , Signature